Chemistry–A European Journal
Research Article
doi.org/10.1002/chem.202301054
Chemistry Europe
European Chemical Societies Publishing
www.chemeurj.org

Special Collection

# Pushing the Boundary of Covalency in Lanthanoid-Tellurium Bonds: Insights from the Synthesis, Molecular and Electronic Structures of Low-Coordinate, Monomeric Europium(II) and Ytterbium(II) Tellurolates

Rajesh Deka,[a, b, c] Sourav Dey,[a] Zhifang Guo,[d] Ray J. Butcher,[e] Peter C. Junk,*[b, d] David R. Turner,[b, c] Harkesh B. Singh,*[a, b] and Glen B. Deacon*[b, c]

**Abstract:** Owing to the strict hard/soft dichotomy between the lanthanoids and tellurium atoms, and the strong affinity of lanthanoid ions for high coordination numbers, low-coordinate, monomeric lanthanoid tellurolate complexes have remained elusive as compared to the lanthanoid complexes with lighter group 16 elements (O, S, and Se). This makes the development of suitable ligand systems for low-coordinate, monomeric lanthanoid tellurolate complexes an appealing endeavor. In a first report, a series of low-coordinate, monomeric lanthanoid (Yb, Eu) tellurolate complexes were synthesized by utilizing hybrid organo-tellurolate ligands containing N-donor pendant arms. The reaction of bis[2-((dimethylamino)methyl)phenyl] ditelluride, **1** and 8,8′diquinolinyl ditelluride, **2** with $Ln^0$ metals ($Ln$ = Eu, Yb) resulted in the formation of monomeric complexes $[Ln^{II}(TeR)_2(Solv)_2]$ [R=$C_6H_4$-2-$CH_2NMe_2$] [**3**: $Ln$ = Eu, Solv = tetrahydrofuran; **4**: $Ln$ = Eu, Solv = acetonitrile; **5**: $Ln$ = Yb, Solv = tetrahydrofuran; **6**: $Ln$ = Yb, Solv = pyridine] and $[Eu^{II}(TeNC_9H_6)_2(Solv)_n]$ (**7**: Solv = tetrahydrofuran, n = 3; **8**: Solv = 1,2-dimethoxyethane, n = 2), respectively. Complexes **3**–**4** and **7**–**8** represent the first sets of examples of monomeric europium tellurolate complexes. The molecular structures of complexes **3**–**8** are validated by single–crystal X-ray diffraction studies. The electronic structures of these complexes were investigated using Density Functional Theory (DFT) calculations, which revealed appreciable covalency between the tellurolate ligands and lanthanoids.

## Introduction

Aside from providing an excellent platform for understanding the lanthanoid ($Ln$)-chalcogen (Ch) bond, lanthanoid chalcogenolate complexes have sparked a great deal of interest due to their advantageous applications in molecular magnetism, precursors for semiconducting materials, catalysis, optics, and electronics.[1] However, lanthanoid complexes with heavier chalcogens (Se, Te) are not very prevalent compared to the analogous species with oxygen or sulfur atoms. This stems from the fact that, according to Pearson's Hard and Soft Acids and Bases (HSAB) principle, lanthanoids are considered to be 'hard' metals and prefer to form complexes with 'hard' ligands.[2] As a result, the synthesis of complexes containing bonds between hard lanthanoid metal ions and soft chalcogen-based ligands is very challenging. Tellurium being the softest and the most electropositive element among group 16 elements, makes its complexation with lanthanoid ions highly unfavorable. It is noteworthy that research on lanthanoid chalcogenolates has predominantly focused on clusters, or oligomers and polymers.[3] This is essentially attributed to the affinity of the lanthanoid ions for high coordination numbers. Additionally, in the case of tellurolate ligand, due to the presence of low-lying lone pair orbitals of Te, the bridging coordination mode is more favorable than for the lighter chalcogenolates. As a result, the synthesis of monomeric lanthanoid tellurolate complexes becomes even more challenging.

[a] R. Deka, S. Dey, H. B. Singh
Department of Chemistry
Indian Institute of Technology Bombay
Mumbai 400076 (India)
[b] R. Deka, P. C. Junk, D. R. Turner, H. B. Singh, G. B. Deacon
IITB-Monash Research Academy
Powai, Mumbai 400076 (India)
[c] R. Deka, D. R. Turner, G. B. Deacon
School of Chemistry
Monash University
Clayton, Victoria 3800 (Australia)
[d] Z. Guo, P. C. Junk
College of Science & Engineering
James Cook University
Townsville 4811, QLD (Australia)
[e] R. J. Butcher
Department of Chemistry
Howard University
Washington, D. C. 20059 (USA)

Supporting information for this article is available on the WWW under https://doi.org/10.1002/chem.202301054

Part of a Special Collection on the p-block elements.

Since f-orbitals have no stereochemical influence on the resulting lanthanoid complex, the bulkiness of the ligands around the metal coordination sphere plays a decisive role in the nuclearity of the complex. As such, the synthesis of monomeric lanthanoid tellurolates is often accomplished by employing a chelating group as an auxiliary ligand or by using an organochalcogenolate ligand with bulky substituent(s).[3d] There are only four crystallographically characterized europium tellurolate compounds deposited with the Cambridge Crystallographic Data Centre (CCDC) as of March 2023, and none of them is monomeric or low-coordinate.[3l,4–6] Similarly, among the monomeric lanthanoid tellurolate complexes reported, the examples of structurally characterized ytterbium tellurolate complexes are fairly rare. Among the five ytterbium tellurolate complexes that have been structurally characterized so far, only three of them are monomers.[6–9] Berg *et al.* have reported the first structurally characterized monomeric ytterbium tellurolate complex, namely $[(Cp^*)_2Yb(TePh)(NH_3)]$, **I**, formed by the reductive cleavage of $Ph_2Te_2$ with $(Cp^*)_2Yb(NH_3)_2$ (Figure 1).[7] Konchenko and co-workers have reported the monomeric complex $[Yb(DippForm)_2(TePh)(THF)]$, **II** [where DippForm = *N,N′*-bis(2,6-diisopropylphenyl)formamidinate, THF = tetrahydrofuran] by the reduction of $Ph_2Te_2$ with $Yb(DippForm)_2(THF)_2$.[8] Brennan and coworkers reported that when $Ph_2Te_2$ was treated with $Yb^0$ in pyridine (py), two phenyltellurolate ligands and five pyridine molecules coordinated to the $Yb^{II}$ centre, producing a hepta-coordinate complex $[(py)_5Yb(TePh)_2]$, **III**.[9] Eu being larger than Yb when reacted with the same phenyltellurolate ligand afforded a 1D coordination polymer $[(THF)_2Eu(\mu\text{-}TeC_6H_5)_2]_\infty$.[4] Thus, it is evident that choosing an appropriate ligand system is highly crucial for synthesizing low-coordinate, monomeric europium tellurolates.

Chelation stabilized organochalcogenolate ligands have received profound interest in stabilizing various chalcogen-based coordination complexes.[10] This class of hybrid ligands, which contain a soft chalcogen atom and a hard donor atom in the auxiliary arm, is particularly useful for isolating monomeric species that would otherwise tend to form polymers or multinuclear complexes through bridging by the chalcogenolate ligands.[10] Here, the hard donor atom from the auxiliary arm, which was previously involved in intramolecular secondary bonding interactions with the chalcogen atom,[11] serves as a chelating arm to the metal centre and results in the formation of a monomeric metal complex. While this approach has been widely used for synthesizing transition metal and main-group chalcogenolates, it is not prevalent in isolating low-coordinate, monomeric lanthanoid chalcogenolates. In the current study, we envisaged using such hybrid ligands for the synthesis of hitherto unknown low-coordinate, monomeric europium tellurolate complexes. As such, we have considered a chelation stabilized pro-ligand, namely bis[2-((dimethylamino)methyl)phenyl] ditelluride, **1** and report the first series of examples of low-coordinate, monomeric europium tellurolate complexes. The viability of such a ligand system is further validated by synthesizing novel examples of low-coordinate, monomeric ytterbium tellurolate complexes. Furthermore, to extend the scope of the reaction we have used a heterocyclic N-donor atom-containing system, namely, 8,8′-diquinolinyl ditelluride, **2** and report a series of monomeric europium tellurolate complexes. Detailed insight into the electronic structural properties of the complexes, particularly with respect to the bonding between the hard *Ln* centre and the soft Te donor atom, has been obtained by Density Functional Theory (DFT) calculations.

## Results and Discussion

### Synthesis and structural characterization

The pro-ligands **1** and **2** were synthesized from *N,N*-dimethylbenzylamine, and 8-bromoquinoline, respectively as reported.[12–13] When the diorgano ditelluride **1** was treated with

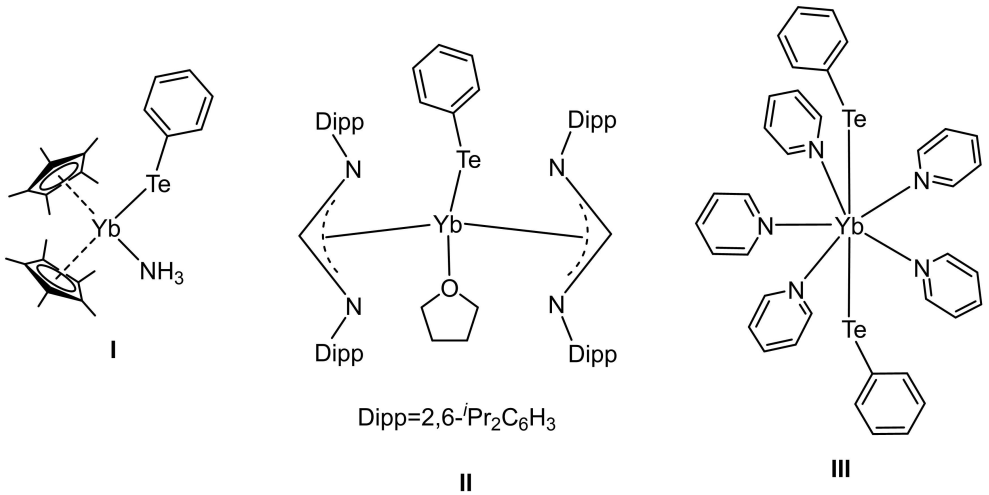


I II III

**Figure 1.** Structurally characterized monomeric ytterbium(II) tellurolates, **I**–**III**.

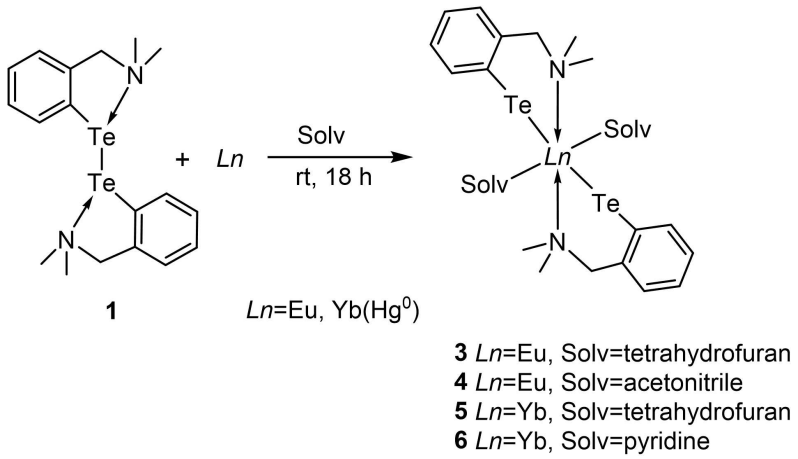


**Scheme 1.** $Eu^{II}$ and $Yb^{II}$ complexes of the 2-((dimethylamino)methyl)phenyltellurolate ligand.

$Eu^0$ metal in THF or acetonitrile, oxidative addition to $Eu^0$ took place and the reaction afforded the first examples of low-coordinate, monomeric europium tellurolate complexes $[Eu^{II}(TeR)_2(Solv)_2]$ [where R=$C_6H_4$-2-$CH_2NMe_2$] [**3**: Solv = THF; **4**: Solv = acetonitrile] (Scheme 1). To determine the generality of this approach, the synthetic method was extended to ytterbium, and the diorgano ditelluride **1** was treated with $Yb^0$ in THF or py under similar reaction conditions. To our expectation, the reactions afforded rare examples of low-coordinate, monomeric ytterbium(II) tellurolate complexes $[Yb^{II}(TeR)_2(Solv)_2]$ [**5**: Solv = THF; **6**: Solv = py], six being low coordinate for lanthanoids. The surfaces of $Yb^0$ metal needed to be activated by a few drops of $Hg^0$ prior to the reaction with **1**.

In line with the foregoing observation, when 8,8′-diquinolinyl ditelluride, **2** was treated with $Eu^0$, a similar oxidative addition reaction took place and resulted in the formation of divalent, monomeric complexes, $[Eu^{II}(TeNC_9H_6)_2(Solv)_n]$ [**7**: Solv = THF, n = 3; **8**: Solv = 1,2-dimethoxyethane (DME), n = 2] (Scheme 2). Unlike the previous case, where the 2-((dimethylamino)methyl)phenyltellurolate ligand yielded hexacoordinated lanthanoid complexes **3**–**6**, the 8-quinolinetellurolate ligand produced complexes with higher coordination numbers (*vide infra*). Thus, the steric effect of this ligand is less than that of **1**, and cannot stabilise a low coordination number.

The molecular structures of complexes **3**–**8** were unambiguously probed by single–crystal X-ray diffraction studies. A comparison of the selected bond lengths and bond angles of the complexes is compiled in Table 1. The salient attribute of the molecular structures of **3**–**8** is a monomeric formulation with two organotellurolate ligands coordinating to the divalent lanthanoid ion in each case. The molecular structures of europium complexes **3** and **4** featuring the 2-((dimethylamino)methyl)phenyltellurolate ligand are shown in Figure 2. Complexes **5** and **6** are isostructural with **3** and **4**, respectively,

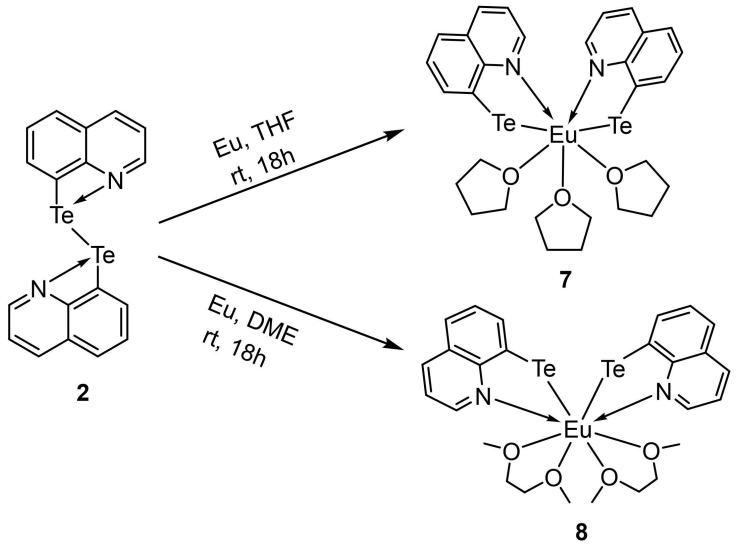


**Scheme 2.** $Eu^{II}$ complexes of the 8-quinolinetellurolate ligand.

**Table 1.** Selected bond lengths (Å) and angles (°) in the crystal structures of complexes 3–8.

| | 3 | 4 | 5 | 6 | 7 | 8 |
|---|---|---|---|---|---|---|
| *Ln*1–Te1 | 3.2576(13) | 3.2258(7) | 3.1611(12) | 3.1534(5) | 3.2717(10) | 3.2691(13) |
| *Ln*1–Te1$^{1}$(/Te2) | 3.2576(14) | 3.2258(7) | 3.1611(12) | 3.1534(5) | 3.3011(10) | 3.2691(13) |
| *Ln*1–N1 | 2.660(3) | 2.677(3) | 2.566(3) | 2.594(4) | 2.683(7) | 2.731(5) |
| *Ln*1–N1$^{1}$(/N2) | 2.660(3) | 2.677(3) | 2.566(3) | 2.594(4) | 2.644(8) | 2.731(5) |
| *Ln*1–D1 | 2.581(3) | 2.653(3) | 2.475(2) | 2.574(4) | 2.559(7) | 2.738(5) |
| *Ln*1–D2 | 2.581(3) | 2.653(3) | 2.475(2) | 2.574(4) | 2.609(7) | 2.661(5) |
| *Ln*1–D3 | | | | | 2.567(7) | 2.738(5) |
| *Ln*1–D4 | | | | | | 2.661(5) |
| Te1–*Ln*1–Te2 | 180 | 180 | 180 | 180 | 176.798(19) | 107.96(4) |
| N1–*Ln*1–N1$^{1}$(/N2) | 180 | 180 | 180 | 180 | 77.9(2) | 123.9(2) |
| N1–*Ln*1–Te1 | 82.62(6) | 80.81(6) | 84.79(6) | 84.00(9) | 67.20(17) | 67.02(11) |
| N1–*Ln*1–Te1$^{1}$(/Te2) | 97.38(6) | 99.19(6) | 95.21(7) | 96.00(9) | 115.98(17) | 80.64(11) |
| N1$^{1}$(/N2)–*Ln*1–Te1 | 97.38(6) | 99.19(6) | 95.21(7) | 96.00(9) | 113.74(17) | 80.64(11) |
| N1$^{1}$(/N2) –*Ln*1–Te1$^{1}$(/Te2) | 82.62(6) | 80.81(6) | 84.79(7) | 84.01(9) | 67.36(17) | 67.02(11) |
| D1–*Ln*1–D2 | 180 | 180 | 180 | 180 | 158.8(2) | 62.22(17) |
| D2–*Ln*1–D3 | | | | | 83.5(2) | 73.31(17) |
| D1–*Ln*1–D3 | | | | | 75.3(2) | 107.1(2) |
| D1–*Ln*1–D4 | | | | | | 73.31(17) |
| D2–*Ln*1–D4 | | | | | | 101.3(3) |

and their molecular structures are included in ESI (Figure S5). In all the complexes **3**–**6**, the hexa-coordinated, divalent lanthanoid ion is on a crystallographically imposed centre of inversion, and so half the structure is generated by symmetry. Each 2-((dimethylamino)methyl)phenyltellurolate ligand fills two coordination sites, one from the soft tellurium atom and the other from the hard nitrogen atom of the pendant arm. Both the N atoms are involved in a six-membered chelate ring at the lanthanoid centre, thereby effectively preventing the molecule from aggregation. The remaining two coordination sites are occupied by two solvent molecules in a *trans* orientation, giving rise to distorted octahedral stereochemistry for the lanthanoid. The *trans* arrangement of the tellurolate ligands is exemplified by ∡(Te–*Ln*–Te1) = 180°, ∡(N–*Ln*–N1) = 180°, and ∡(D–*Ln*–D1) = 180° (where D = donor atom of the solvent molecule). The nitrogen donor atom of the pendant arms furnishes an N–*Ln*–Te bite angle close to 90° in all cases (Table 1). The smaller ionic radius of Yb$^{II}$ in comparison to the Eu$^{II}$ ion causes a N–*Ln*–Te smaller bite angle in complexes **5** and **6** than in **3** and **4**.

In the molecular structure of complexes **3** and **4**, the Eu–Te bond lengths are 3.2576(13) Å and 3.2576(14) Å (**3**) and 3.2258(7) Å (**4**). These values are significantly smaller than the Eu–Te bond lengths of the 1D polymer $[(THF)_2Eu(TeC_6H_5)_2]_\infty$ [3.335(2)–3.359(2) Å].[4] This is because, in the 1D polymer, Eu ions are bridged through Te atoms, thereby lengthening the Eu–Te bonds. In the case of complexes **5** and **6**, the Yb–Te bond lengths [3.1611(12) and 3.1534(5) Å, respectively] are shorter than in the hepta-coordinated ytterbium tellurolate complex **III** [3.248(1) and 3.315(1) Å] by more than the 0.06 Å expected[14] for a change in coordination number from 6 to 7. Again, according to Shannon's radii, the difference in the ionic radii of Eu$^{II}$ and Yb$^{II}$ for coordination number 6 is 0.15 Å.[14] However, the observed change in *Ln*–Te bond lengths from the europium tellurolate complexes (**3** and **4**) to the ytterbium tellurolate complexes (**5** and **6**) is 0.06–0.10 Å. Possibly, the increased steric stress caused by the decrease in atomic radius

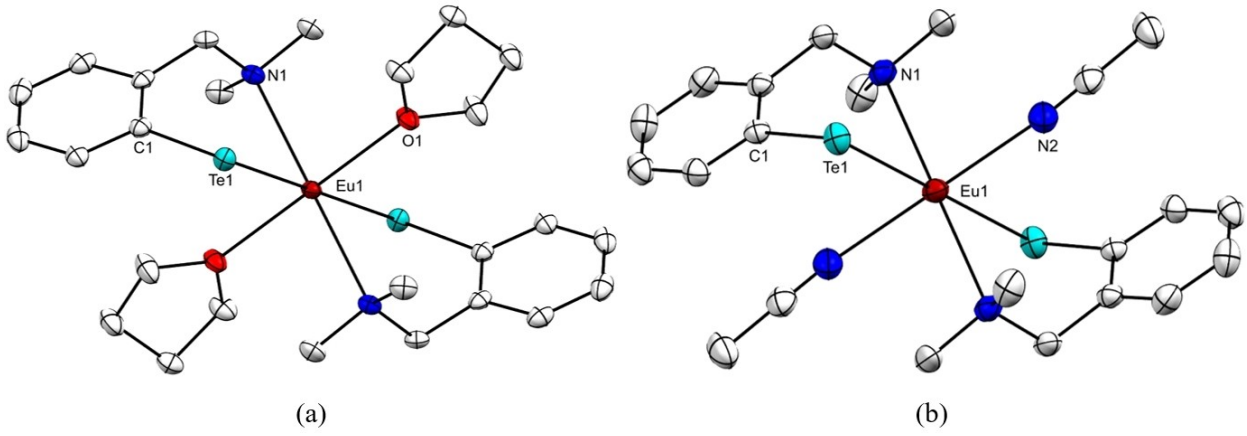


**Figure 2.** Molecular structures of (a) **3** and (b) **4**; thermal ellipsoids are set at the 50% probability level.

from $Eu^{II}$ to $Yb^{II}$ prevents the expected contraction of the Yb–Te bonds in complexes **5** and **6**.

The molecular structures of complexes **7** and **8** are shown in Figure 3. Interestingly, in the THF solution, the reaction with 8,8′-diquinolinyl ditelluride ligand afforded a hepta-coordinated europium complex $[Eu^{II}(TeNC_9H_6)_2(THF)_3]$ **7**, whereas, in DME, an octa-coordinated complex $[Eu^{II}(TeNC_9H_6)_2(DME)_2]$ **8** was obtained. An explanation for the formation of the octa-coordinated complex with DME can be found by considering the steric coordination number ($CN_s$) of the two DME molecules, which is almost the same as that of three THF molecules [$CN_s$ (THF) = 1.21; $CN_s$ (DME) = 1.78].[15] Unlike in complexes **3**–**6**, the nitrogen atoms of the quinoline moiety in complexes **7** and **8** furnish five-membered chelate rings. In complex **7**, the two 8-quinolinetellurolate ligands occupy the axial (*trans*) positions [∡(Te1–Eu–Te2) = 176.798(19)°]. The three THF molecules make a T-shape arrangement around the $Eu^{II}$ centre. The two nitrogen donor atoms from the tellurolate ligands are cis [∡(N1–Eu1–N2) = 77.9(2)°]. Contrastingly, a different spatial arrangement of the 8-quinolinetellurolate ligands is observed in complex **8**, as evident from the difference in Te1–Eu1–Te2 [107.96(4)°] and N1–Eu1–N2 [123.9(2)°] angles. In complex **8**, the octa-coordinated $Eu^{II}$ ion is on a crystallographically imposed inversion centre. The Eu–Te bond lengths in **7** [3.2717(10) and 3.3011(10) Å] and **8** [3.2691(13) Å] are slightly longer than observed for **3** and **4**, consistent with the increase in coordination number. The N–Eu–Te bite angles in complex **7** are found to be 67.20(17)° and 67.36(17)°. A similar bite angle [67.02(11)°] is observed in **8**.

This should be a footnote to Table 1Due to the paramagnetic nature of $Eu^{II}$, and excessive broadening and shifting of the resonances, no satisfactory $^1$H NMR spectra were obtained for complexes **3**–**4** and **7**–**8**. For diamagnetic $Yb^{II}$ complexes **5** and **6**, the $^1$H and $^{13}$C NMR spectra, recorded in benzene-$d_6$, showed a single set of resonance signals which were assigned to the '$C_6H_4$-2-$CH_2NMe_2$' moiety and a solvent [**5**, THF; **6**, py] molecule in a 1:1 ratio (Figure S1–S4, ESI). In particular, the $^1$H NMR spectra of **5** and **6**, showed sharp singlets at ~2.0 ppm corresponding to the methyl protons from the *N,N*-dimethylbenzylamine moiety. The methylene protons attached to the $-NMe_2$ showed a sharp singlet at ~3.2 ppm, indicating a fast-conformational change of the six-membered chelating ring on the NMR time scale. Such a fluxional behavior of the flanking $-NMe_2$ arm in solution state at room temperature has also been reported for related organochalcogenolate complexes, such as in $[M\{EC_6H_4\text{-}2\text{-}CH_2NMe_2\}\{N(SiMe_3)_2\}]$ (where M=Ge, Sn, Pd; E=S, Se), $[In\{SC_6H_4\text{-}2\text{-}CH_2NMe_2\}_3]$, $[M\{SeC_6H_4\text{-}2\text{-}CH_2NEt_2\}_2]$ (where M=Zn, Cd), $[Hg\{SeC_6H_4\text{-}2\text{-}CH_2NMe_2\}_2]$, $[Hg_2\{SeC_6H_3\text{-}2,6\text{-}(CH_2NMe_2)_2\}Cl_3]$, $[AlCl_2\{S(C_6H_3\text{-}2\text{-}CH_2NC_5H_{10}\text{-}5\text{-}^tBu)\}$ $-\kappa^2S,N]$, and $[AlCl_2\{S(SiMe_3)(C_6H_3\text{-}2\text{-}CH_2NMe_2\text{-}5\text{-}^tBu)\}-\kappa^2S,N]$.[16] Within half an hour, precipitation was observed in the NMR tube, indicating that the complexes were not stable for a long period in $C_6D_6$. A similar observation was made by Brennan and coworkers for complex **III**, which they attributed to the formation of a coordination polymer with indefinite composition.[9] Attempts to re-dissolve the precipitate in common organic solvents were unsuccessful, indicating that the precipitation was irreversible. This also precluded the low-temperature NMR measurement of complexes **5** and **6**. The formulations of the bulk complexes were established by elemental analyses which match well with their respective single–crystal X-ray diffraction compositions.

## Computational Studies

To delve into the exact nature of bonding between the *Ln* and Te in complexes **3**–**8**, the electronic structures of the complexes have been studied by DFT calculations with the Gaussian 0.9 (Rev A.02) program[17] [functional: UB3LYP;[18] mixed basis set: Te: SDD effective core potential;[19] C/H/N/O: SVP; [20] *Ln* (Yb, Eu): Cundari–Stevens double-ζ polarization[21]]. After a geometry

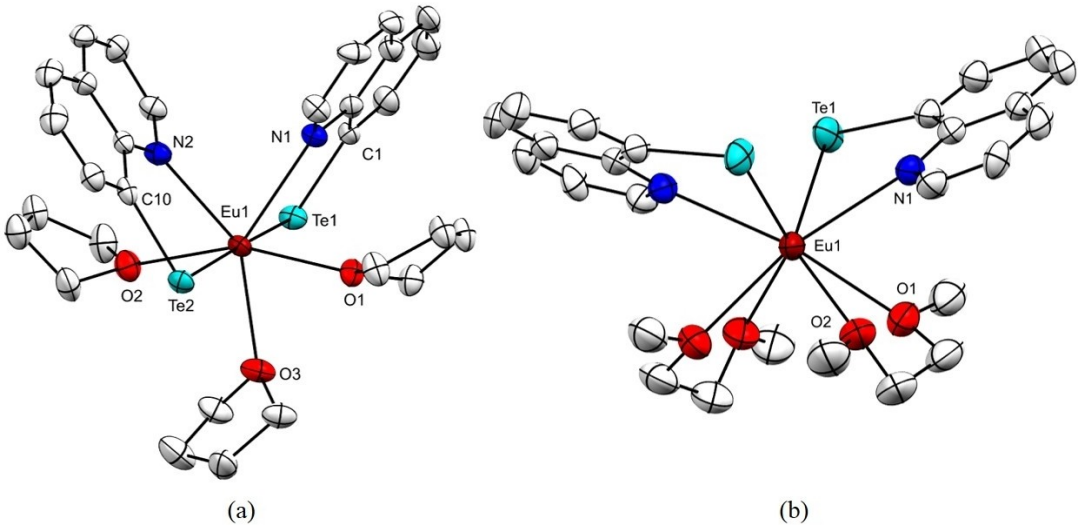


**Figure 3.** Molecular structures of (a) **7** and (b) **8**; thermal ellipsoids are set at the 50% probability level.

optimization starting from the crystal coordinates, Natural Bond Orbital (NBO)/Natural Localized Molecular Orbital (NLMO) calculations were performed. The advantageous features associated with NBO/NLMO analysis, such as the use of non-degenerate occupancies, maintenance of compulsive orthonormality, and omission of un-assignable overlap densities; make it a powerful diagnostic tool to explore the nature of metal–ligand bonding in a complex.[22] The examination of NLMOs reveals that each *Ln*–Te bond exhibits a similar level of polarization in complexes **3**–**8** (Figure 4). In particular, the percentage metal atom (%M) contribution in each *Ln*–Te bond lies in the range of 9.07–10.64 (%M). The Te atom adds up the remainder contribution which ranges between 90.93–89.36 (%M). The breakdown of the NLMOs of the *Ln*–Te bonding interaction indicates that while in all cases, the Te orbital is predominantly p character (~91%) in nature with a minor s contribution (~9%), the metal uses a hybrid orbital consisting of s, p, and d character. In particular, in the cases of **3**–**6**, the p orbital accounts for nearly half of the metal contribution, while the s and d orbitals provide nearly 20% and 30% of the meal contribution, respectively. A slight disparity was observed in the orbital composition of **7** and **8**. The Eu component in complex **7** is made up of 19% s, 47% p, and 34% d characters. In complex **8**, the Eu component is composed of 18% s, 36% p, and 46% d characters. The representative NLMO plots of the *Ln*–Te bond and the orbital composition of the *Ln* and Te atoms are shown in Figure 5. From the studies it can be inferred that although the *Ln*–Te bonds in the complexes are mostly localized on the Te atoms, the lanthanoid metal has an important contribution to the bond, resulting in noticeable covalency in the bond. Based on Mulliken charges calculated for complexes **3**–**8**, the central metal ions bear positive charges ranging from 0.99 to 1, while the tellurolate ions bear negative charges between −0.24 and −0.25 (Figure S12, ESI). Such a dissipation of charges indicates noticeable electron sharing between the central metal ions and the tellurolate ligands in the complexes.

The sharing of electrons between the lanthanoid and the tellurium atom in **3**–**8** was further validated by Electron Localization Function (ELF) studies, which provide a mapping of localized electron pairs across a bond.[23] The ELF plot for complex **3** is shown in Figure 6(a). For complexes **4**–**8**, the corresponding ELF plots are included in the ESI (Figure S13). In all the complexes, a continuum of elevated ELF values was observed along each *Ln*→Te vector, indicating effective overlap of lanthanoid orbitals with Te donor orbitals.

To gain quantitative insights about *Ln*–Te bonds and corroborate the findings of NBO and ELF analyses, the topological properties of *Ln*–Te bond critical points (BCPs) in complexes **3**–**8** were investigated by Quantum Theory of Atoms in Molecules (QTAIM) analysis.[24] The topological parameters of the *Ln*–Te BCPs for complex **3**–**8** are compiled in Table 2. The contour line diagram of the Laplacian of electron density, $\nabla^2\varrho(r)$ plot for complex **3** is shown in Figure 6(b). The corresponding $\nabla^2\varrho(r)$ plots for complexes **4**–**8** are included in the ESI (Figure S14). The analysis of the topological parameters of the *Ln*–Te bonds indicated that magnitudes of electron density $\varrho(r)$, which measures the accumulation of charge along a bond path, lie in the range 0.0223–0.0237 eÅ$^{-3}$. The corresponding total energy density values, H(r) are negative with $|H(r)|$ values ranging from $0.108\times10^{-2}$–$0.765\times10^{-2}$ eÅ$^{-3}$. These values indicate the presence of appreciable covalent character in the *Ln*–Te bond. This is further corroborated by the magnitude of $|V(r)|/G(r)$ ratios, which are in the range of 1.05–1.13, indicating a mixed character, *i.e.*, predominantly ionic with a noticeable covalent component, of the *Ln*–Te bond.[24b–c] Thus, QTAIM analyses correlate well with the NBO/NLMO analyses and provide a unified description of metal-ligand covalency in complexes **3**–**8**.

This should be footnote to Table 2The frontier molecular orbitals (FMOs) for complexes **3**–**8** are shown in Figure 7. The plots of FMOs reveal that in complexes **3**–**6** featuring the 2-((dimethylamino)methyl)phenyltellurolate ligand, the highest occupied molecular orbital (HOMO) is mostly centred on $p_x$ and

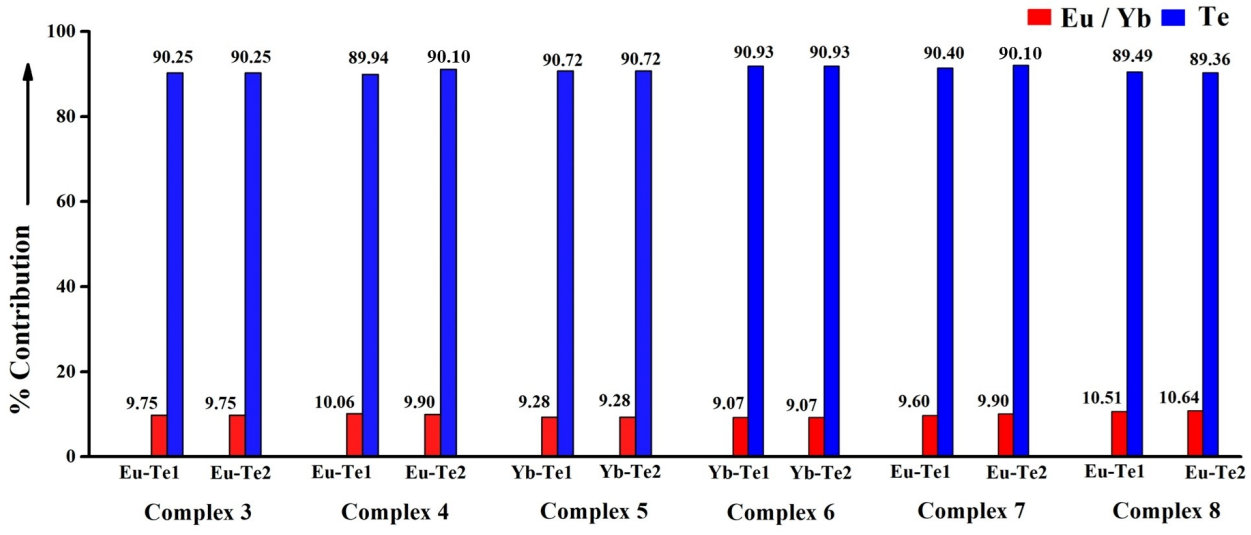


**Figure 4.** The relative contribution of *Ln* (Eu/Yb) and Te in the *Ln*–Te bond in complexes **3**–**8** as calculated by NBO/NLMO study.

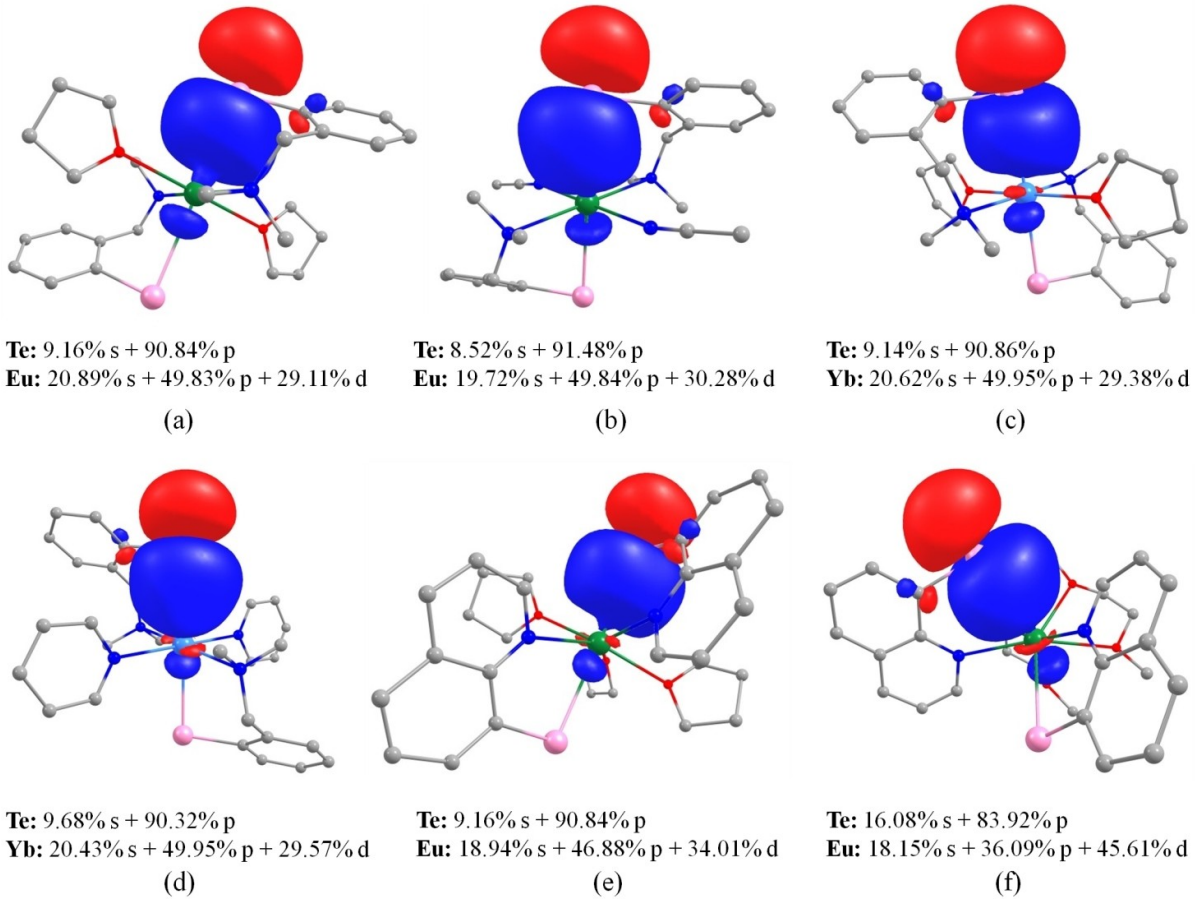


**Figure 5.** Representative NLMO plots of *Ln*–Te bonding interactions and their composition in (a) **3**, (b) **4**, (c) **5**, (d) **6**, (e) **7**, and (f) **8**. The NLMO has been shown with an isosurface value of 0.02 $e^{-}$/bohr$^3$.

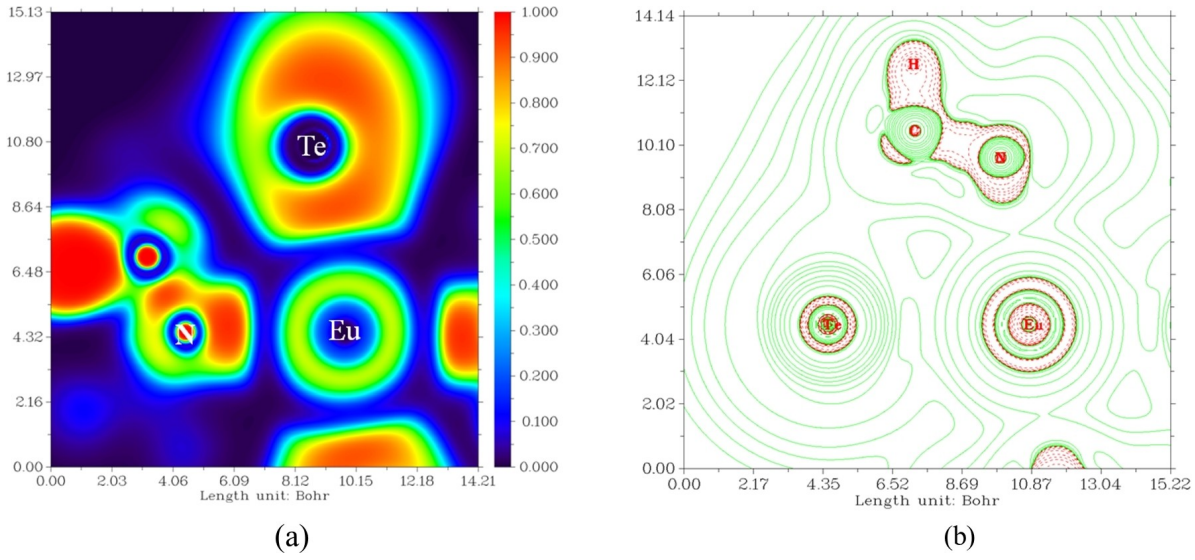


**Figure 6.** (a) Electron localization function (ELF) for **3** drawing in the plane containing N, Te, and Eu atoms, (b) Contour line diagram of the Laplacian of electron density, $\nabla^2\varrho(r)$ along the *Ln*–Te plane for complex **3**.

**Table 2.** Topological parameters at BCPs in the Ln–Te bonds of complexes **3**–**8**. ϱ(r) in units of eÅ$^{-3}$.

| Complex | Bond | ϱ(r) | $\nabla^2$ϱ(r) | ε | V(r) | G(r) | H(r) | \|V(r)\|/G(r) |
|---|---|---|---|---|---|---|---|---|
| **3** | Eu–Te1 | 0.0233 | 0.0435 | 0.158 | −0.0139 | 0.0123 | −0.00157 | 1.13 |
| | Eu–Te2 | 0.0233 | 0.0435 | 0.148 | −0.0139 | 0.0123 | −0.00157 | 1.13 |
| **4** | Eu–Te1 | 0.0237 | 0.0450 | 0.162 | −0.0144 | 0.0127 | −0.00165 | 1.13 |
| | Eu–Te2 | 0.0233 | 0.0450 | 0.162 | −0.0144 | 0.0127 | −0.00165 | 1.13 |
| **5** | Yb–Te1 | 0.0229 | 0.0515 | 0.141 | −0.0143 | 0.0135 | −0.000765 | 1.06 |
| | Yb–Te2 | 0.0229 | 0.0515 | 0.141 | −0.0143 | 0.0135 | −0.000765 | 1.06 |
| **6** | Yb–Te1 | 0.0223 | 0.0507 | 0.134 | −0.0138 | 0.0131 | −0.000626 | 1.05 |
| | Yb–Te2 | 0.0223 | 0.0507 | 0.134 | −0.0138 | 0.0131 | −0.000626 | 1.05 |
| **7** | Eu–Te1 | 0.0224 | 0.0450 | 0.147 | −0.0135 | 0.0123 | −0.00118 | 1.10 |
| | Eu–Te2 | 0.0224 | 0.0450 | 0.147 | −0.0135 | 0.0123 | −0.00118 | 1.10 |
| **8** | Eu–Te1 | 0.0223 | 0.0448 | 0.148 | −0.0132 | 0.0121 | −0.00108 | 1.09 |
| | Eu–Te2 | 0.0224 | 0.0448 | 0.148 | −0.0132 | 0.0122 | −0.00109 | 1.09 |

$p_y$ orbitals of the Te atoms. In contrast, there is quite a disparity in the nature of the lowest occupied molecular orbitals (LUMO) among the complexes. In particular, in complex **3**, the LUMO is composed of an s orbital of the N atom and $p_x+p_y$ orbitals of the carbon atoms of the organyl substrate. In complex **4**, on the other hand, the LUMO is a hybrid orbital composed of the s+d orbitals of Eu and the $p_x+p_y$ orbitals of C and N atoms. Again, in complex **5**, the LUMO is localized on the $p_x+p_y$ orbitals of the C atoms, whereas in complex **6**, the LUMO is localized on the $p_x+p_y$ orbitals of both the N and C atoms. In the case of complex **7** featuring 8-quinolinetellurolate ligand, the HOMO is composed of $p_x+p_y$ of Te and an s+p combination of C atoms. The corresponding LUMO is localized on the $p_x+p_y$ orbitals of the N atoms and $p_x+p_y+p_z$ orbitals of the C atoms. In complex **8**, the HOMO is composed of $p_x+p_y$ orbitals of C and N atoms. The LUMO is centred on the s+d+f orbitals of Eu, an s orbital of C, and p orbitals of N atoms. The energy gaps between the HOMO and the LUMO in complexes **3**–**6** are in the range of 3.07–4.29 eV, while the corresponding energy gaps in complexes **7** and **8** are in the range of 2.67–2.73 eV. Due to the high magnitude of the HOMO-LUMO gaps, it is energetically unfavorable to add electrons to a LUMO which is lying at a high energy level from a deep-lying HOMO.[25]

## Conclusions

Despite the intriguing structural and bonding aspects, and promising applications of lanthanoid chalcogenolates, the synthesis of low-coordinate monomeric lanthanoid tellurolate remains a challenging endeavor. Although the molecular structure of multinuclear europium tellurolate complexes has been known since 1994,[4] the monomeric low-coordinate counterpart was still elusive. This study presents the first set of structurally characterized low-coordinate, monomeric europium tellurolate complexes (**3**—**4**) by utilizing a chelation stabilized organotellurolate ligand namely, 2-((dimethylamino)methyl)-phenyltellurolate. The synthesis of two low-coordinate, monomeric ytterbium tellurolate complexes **5**—**6** was also accomplished with the same ligand. For a comparison, when a heterocyclic N-donor atom containing ligand, namely 8-quinolinetellurolate, is used, the change in N–*Ln*–Te bite angle as well as reduced crowding around the nitrogen arm results in the isolation of hepta- and octa-coordinated complexes **7** and **8**. All complexes were prepared by reactions between the free lanthanoid metal and the appropriate ditelluride. The molecular structures of the complexes reveal that the N→*Ln* interactions, along with the steric bulk of the ligands, prevent the formation of higher-order aggregates and facilitate the isolation of the desired monomeric species. The HOMO-LUMO energy gaps in the complexes are significantly high, indicating that the complexes are kinetically stable. The %M contribution obtained from the NBO/NLMO analysis; together with the topological parameters of *Ln*–Te BCPs indicates sharing of electrons between the metal centre and the tellurolate ligands, resulting in significant covalency in the bond. As secondary bonding interaction stabilized heavier dichalcogenides are well known,[10,26] the present approach has the potential to open up a wide range of new lanthanoid tellurolate complexes. Since the magnetism of europium chalcogenides has received significant attention in recent years,[27] monomeric europium tellurolate species offer alternative prospects in molecular magnetism.

## Experimental Section

**General**: The lanthanoid compounds synthesized are highly air and moisture-sensitive and were prepared and handled with vacuum-nitrogen line techniques and in an Mbraun glove box, under an atmosphere of purified nitrogen. The starting materials and solvents were purchased from commercial sources. Bis[2-((dimethylamino)-methyl)phenyl] ditelluride, **1** was synthesized following a reported procedure.[12] Treatment of *N,N*-dimethylbenzylamine with $^n$BuLi followed by the addition of tellurium powder and subsequent oxidation afforded compound **1**. 8,8′-diquinolinyl ditelluride, **2** was synthesized by reacting 8-bromoquinoline with *in-situ* generated disodium ditelluride, $Na_2Te_2$.[13] Lanthanoid chunks were freshly filed in the Glove box before use. Solvents (THF, DME) were pre-dried with sodium metal and then further dried by distillation over sodium or sodium/benzophenone, and were degassed (by freeze-pump-thaw) prior to use. Acetonitrile was distilled from calcium hydride, degassed, and stored over dried 3 Å molecular sieves. Pyridine was distilled from potassium hydroxide, degassed, and stored over dried 4 Å molecular sieves. NMR solvent, $C_6D_6$ was degassed and dried over sodium with stirring overnight and filtered before use. IR spectra were recorded as Nujol mulls between NaCl plates using a transmittance IR instrument within the range 4000–600 cm$^{-1}$. $^1$H (400

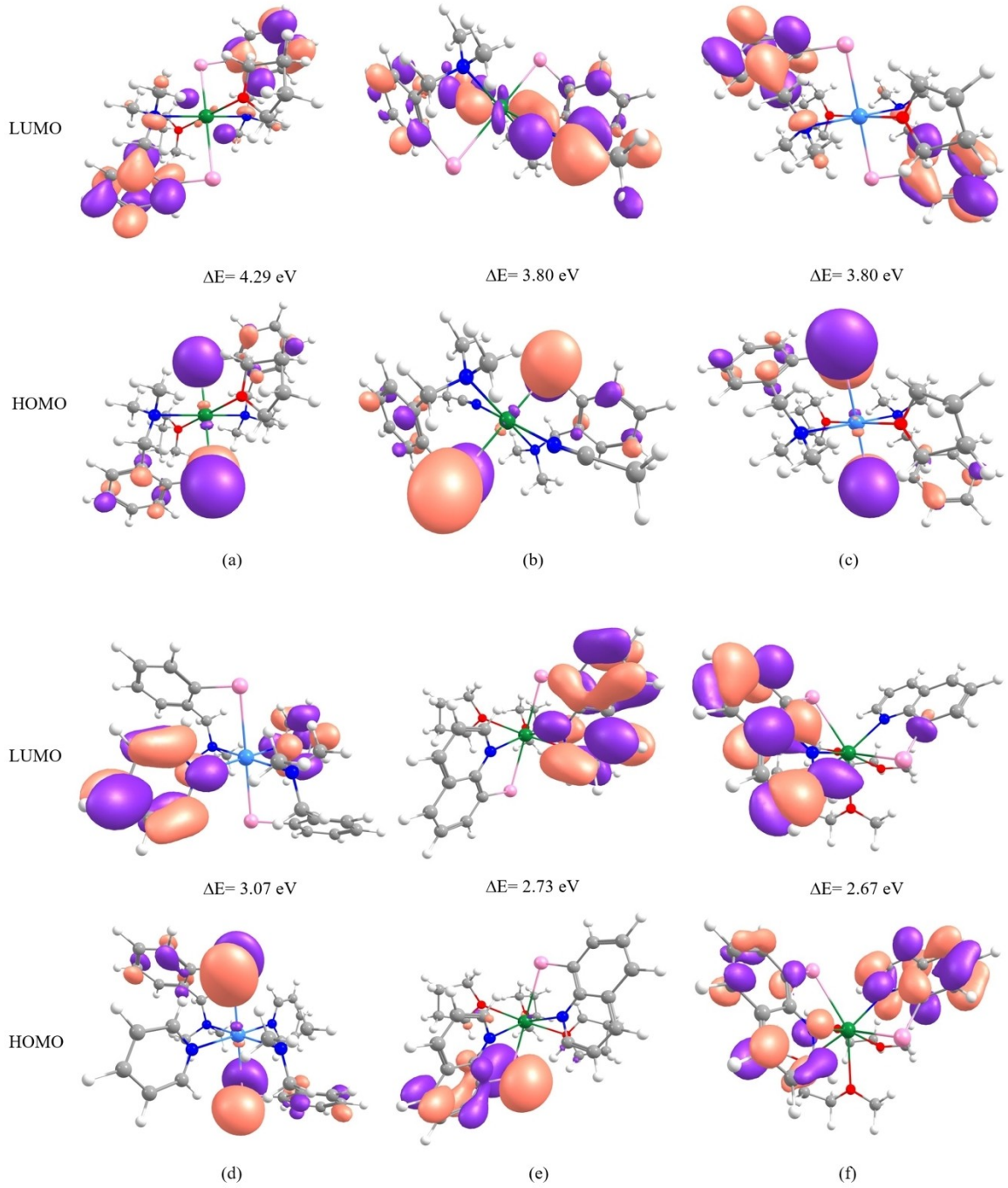


**Figure 7.** Frontier molecular orbital (FMO) plots of complexes (a) **3**, (b) **4**, (c) **5**, (d) **6**, (e) **7**, and (f) **8** and their HOMO-LUMO energy gaps.

and 500 MHz), $^{13}C$ (100 and 125 MHz) NMR spectra were recorded on Bruker AV 400 MHz and Bruker AV 500 MHz spectrometers at 25 °C. The chemical shifts cited were referenced to TMS ($^{1}H$, $^{13}C$) as external standards. Microanalysis sample were sealed in glass ampoules under purified nitrogen and were determined by the Elemental Analysis Service (London Metropolitan University) or on a Carlo Erba model 1106 elemental analyser (IITB). Melting points were determined in sealed glass capillaries under nitrogen and are uncalibrated.

**Computational details**: Geometry optimization followed by single-point calculation of complex **3**–**8** were conducted with the Gaussian 0.9 (Rev A.02) package.[17] The UB3LYP functional along with Cundari–Stevens double-ζ polarization basis set for Eu and Yb and the SDD basis set for Te, SVP basis set for C, H, N, O were used.[18–21] The NBO/NLMO analysis was carried out with the optimized structures of complexes **3**–**8**. Frequency calculations were performed, and all the structures were detected with minima such that no negative frequencies were observed. The topological and ELF analyses were carried out with Multiwfn software.[28]

**X-ray crystallography**: Crystals were immersed in crystallography oil and were measured on MX1 macromolecular beamline at the Australian Synchrotron,[29] where the data collection and integration were completed using the *Blu-ice*[30] and *XDS*[31] software programs,

respectively. The structures were solved using direct methods and refined with least-squares methods against $F^2$, using *SHELXS* and *SHELXL* respectively,[32] with *Olex2*[33] used as a graphical interface. All non-hydrogen atoms were refined using an anisotropic model and all hydrogen atoms were refined using a riding model in idealized geometries. Crystallographic data are presented in Table S1.

Deposition Number(s) 2142908 (**3**), 2142909 (**4**), 2142910 (**5**), 2142911 (**6**), 2142912 (**7**) and 2142913 (**8**) contain(s) the supplementary crystallographic data for this paper. These data are provided free of charge by the joint Cambridge Crystallographic Data Centre and Fachinformationszentrum Karlsruhe Access Structures service.

**General procedure for the synthesis of 3–8**: In a Schlenk flask, lanthanoid metal fillings (4.0 mmol) and the diorgano ditelluride (1.0 mmol) were taken in an appropriate solvent (*ca.* 20 mL) and the reaction mixture was stirred for 18 h at room temperature. The reaction mixture was filtered through a filtering cannula to remove the excess metal. The volume of the filtrate was reduced under vacuum to *ca.* 10 mL and the flask was stored at −30 °C. Crystals were obtained after 20–30 days and examined by single-crystal X-ray diffraction studies.

**Note**: In the case of complexes **5** and **6**, two drops of $Hg^0$ were added to Yb filings in 10 mL of the corresponding solvent and were allowed to stir for 1 h prior to the addition of the diorgano ditelluride.

**[$Eu^{II}${$TeC_6H_4$-2-$CH_2NMe_2$}$_2$($THF)_2$]**, **3**: Yellow crystals; Yield: 74%; m.p. 158–159 °C; Anal. Calc. (%) for $C_{26}H_{40}EuN_2O_2Te_2$ (819.782): C 38.09, H 4.92, N 3.42; found C 37.91, H 4.86, N 3.41; IR (Nujol, $cm^{-1}$): $\bar{\upsilon}$ 3038 (w), 2957 (s), 2925 (s), 2856 (s), 2782 (w), 2414 (w), 2272 (w), 1884 (w), 1577 (m), 1457 (s), 1374 (m), 1313 (w), 1246 (m), 1174 (m), 1023 (s), 950 (w), 918 (m), 868 (m), 835 (m), 800 (s), 751 (s).

**[$Eu^{II}${$TeC_6H_4$-2-$CH_2NMe_2$}$_2$(MeCN)$_2$]**, **4**: Yellow crystals; Yield: 79%; m.p. 161–162 °C; Anal. Calc. (%) for $C_{22}H_{30}EuN_4Te_2$ (757.674): C 34.88, H 3.99, N 7.39; found C 35.23, H 3.78, N 7.43; IR (Nujol, $cm^{-1}$): $\bar{\upsilon}$ 2920 (m), 2833 (w), 1619 (w), 1499 (s), 1456 (m), 1359 (w), 1275 (s), 1232 (w), 1128 (s), 1091 (m), 1039 (m), 941 (m).

**[$Yb^{II}${$TeC_6H_4$-2-$CH_2NMe_2$}$_2$($THF)_2$]**, **5**: Orange crystals; Yield: 85%; m.p. 178 °C; $^1$H NMR (400 MHz, $C_6D_6$): δ 7.30–7.27 (m, 4H), 7.15–7.12 (m, 2H), 7.09–7.04 (m, 2H), 3.56–3. 52 (m, 8H), 3.22 (s, 4H), 2.04 (s, 12H), 1.43–1.39 (m, 8H); $^{13}$C NMR (100 MHz, $C_6D_6$): δ 139.6, 128.7, 127.9, 127.7, 127.4, 126.8, 67.4, 64.2, 45.0, 25.4; Anal. Calc. (%) for $C_{26}H_{40}YbN_2O_2Te_2$ (840.863): C 37.14, H 4.80, N 3.33; found C 37.29, H 4.93, N 3.19; IR (Nujol, $cm^{-1}$): $\bar{\upsilon}$ 2924 (s), 2854 (s), 2781 (w), 2723 (w), 2283 (w), 1578 (m), 1457 (m), 1374 (w), 1260 (m), 1094 (m), 1021 (m), 841 (w), 799 (m), 746 (w).

**[$Yb^{II}${$TeC_6H_4$-2-$CH_2NMe_2$}$_2$(py)$_2$]**, **6**: Red crystals; Yield: 85%; m.p. 174–177 °C; $^1$H NMR (500 MHz, $C_6D_6$): δ 8.52–8.51 (m, 4H), 7.34–7.32 (dd, $J$ = 7.6, 1.7 Hz, 4H), 7.20–7.18 (m, 2H), 7.11–7.08 (m, 2H), 7.03–6.99 (m, 2H), 6.70–6.67 (m, 4H), 3.25 (s, 4H), 2.07 (s, 12H); $^{13}$C NMR (126 MHz, $C_6D_6$): δ 149.9, 139.6, 134.9, 128.8, 127.9, 127.7, 127.5, 126.9, 123.2, 64.2, 45.1; Anal. Calc. (%) for $C_{28}H_{34}YbN_4Te_2$ (854.853): C 39.34, H 4.01, N 6.55; found C 39.11, H 4.17, N 6.89; IR (Nujol, $cm^{-1}$): $\bar{\upsilon}$ 2924 (s), 2855 (s), 2728 (w), 2313 (w), 1595 (w), 1460 (m), 1377 (w),1261 (w), 1147 (w), 1029 (w), 743 (w), 702 (w).

**[$Eu^{II}$($TeNC_9H_6$)$_2$($THF)_3$]**, **7**: Yellow crystals; Yield: 72%; m.p. 187 °C; Anal. Calc. (%) for $C_{30}H_{36}EuN_2O_3Te_2$ (879.793): C 40.96, H 4.12, N 3.18; found C 40.82, H 4.20, N 3.25; IR (Nujol, $cm^{-1}$): $\bar{\upsilon}$ 2924 (s), 2856 (s), 2684 (w), 2414 (w), 2317 (w), 1795 (w), 1663 (w), 1586 (m), 1486 (m), 1457 (s), 1413 (m), 1376 (m), 1288 (m), 1205 (m), 1126 (m), 1064 (m), 1034 (s), 959 (m), 892 (m), 825 (m), 792 (m).

**[$Eu^{II}$($TeNC_9H_6$)$_2$($DME)_3$]**, **8**: Yellow crystals; Yield: 76%; m.p. 191–192 °C; Anal. Calc. (%) for $C_{26}H_{32}EuN_2O_4Te_2$ (843.716): C 37.01, H 3.82, N 3.32; found C 37.09, H 4.01, N 2.97; IR (Nujol, $cm^{-1}$): $\bar{\upsilon}$ 2924 (s), 2855 (m), 1595 (w), 1453 (m), 1372 (w), 1297 (w), 1261 (w), 1200 (w), 1114 (w), 1066 (m), 1024 (w), 954 (w), 858 (w), 819 (m), 785 (m).

## *Acknowledgements*

The authors would like to acknowledge the Department of Science and Technology (DST), India (J. C. Bose Fellowship 15DSTFLS002, Grant No. RD/0115-DSTFLS80-004) and IITB-Monash Research Academy (IMURA 0242) for providing funding to carry out this research. R. D. thanks Dr. Rory Kelly, Violina Sarmah, and Suman Dhara for their technical support. S. D. acknowledges UGC for SRF. We acknowledge the Supercomputing facility of IIT Bombay, Space Time-2, for computational studies. PCJ and GBD gratefully acknowledge the Australian Research Council for funding (DP190100798 and DP230100112). Parts of this research were undertaken on the MX1 beamline at the Australian Synchrotron, part of ANSTO.[29] Open Access publishing facilitated by James Cook University, as part of the Wiley - James Cook University agreement via the Council of Australian University Librarians.

## Conflict of Interests

The authors declare no conflicts of interest.

## Data Availability Statement

Spectroscopic data (for **5** and **6**), supplementary figures and tables, and cartesian coordinates for **3**–**8** can be found in the ESI. The data that support the findings of this study are available from the corresponding author upon reasonable request.

**Keywords:** europium · lanthanoid · low-coordinate · monomer · tellurium

[1] a) M. D. Regulacio, K. Bussmann, B. Lewis, S. L. Stoll, *J. Am. Chem. Soc.* **2006**, *128*, 11173–11179; b) J. Y. Kim, T. Livinghouse, *Org. Lett.* **2005**, *7*, 1737–1739; c) S. Arndt, A. Trifonov, T. P. Spaniol, J. Okuda, M. Kitamura, T. Takahashi, *J. Organomet. Chem.* **2002**, *647*, 158–166; d) K. Kuriki, Y. Koiki, Y. Okamoto, *Chem. Rev.* **2002**, *102*, 2347–2356; e) G. A. Kumar, R. E. Riman, S. Chen, D. Smith, J. Ballato, S. Banerjee, A. Kornienko, J. G. Brennan, *Appl. Phys. Lett.* **2006**, *88*, 91902–91903; f) A. Kornienko, S. Banerjee, G. A. Kumar, R. E. Riman, T. J. Emge, J. G. Brennan, *J. Am. Chem. Soc.* **2005**, *127*, 14008–14014; g) G. A. Kumar, R. E. Riman, L. A. D. Torres, O. B. Garcia, S. Banerjee, A. Kornienko, J. G. Brennan, *Chem. Mater.* **2005**, *17*, 5130–5135; h) A. R. Strzelecki, C. L. Likar, B. A. Helsel, T. Utz, M. C. Lin, P. A. Bianconi, *Inorg. Chem.* **1994**, *33*, 5188–5194; i) A. R. Strzelecki, P. A. Timinski, B. A. Helsel, P. A. Bianconi, *J. Am. Chem. Soc.* **1992**, *114*, 3159–3160; j) A. Tcakaev, V. B. Zabolotnyy, C. I. Fornari, P. Rüßmann, R. F. Peixoto, F. Stier, M. Dettbarn, P. Kagerer, E. Weschke, E. Schierle, P. Bencok, P. H. O. Rappl, E. Abramof, H. Bentmann, E. Goering, F. Reinert, V. Hinkov, *Phys. Rev.* **2020**, *B 102*, 184401; k) A. J. Gaunt, S. D. Reilly, A. E. Enriquez, B. L. Scott, J. A. Ibers, P. Sekar, K. I. M. Ingram, N. Kaltsoyannis, M. P. Neu, *Inorg. Chem.* **2008**, *47*, 29–41; l) N. A. G. Gray, J. S. Price, D. J. H. Emslie, *Chem. Eur. J.* **2022**, *28*, e202103580.

[2] a) R. G. Pearson, *J. Am. Chem. Soc.* **1963**, *85*, 3533–3539; b) R. G. Pearson, *J. Chem. Educ.* **1968**, *45*, 581–587; c) R. G. Pearson, *J. Chem. Educ.* **1968**, *45*, 643–648.
[3] a) G. A. Kumar, R. E. Riman, J. G. Brennan, *Coord. Chem. Rev.* **2014**, *273–274*, 111–124; b) W. Boncher, H. Dalafu, N. Rosa, S. Stoll, *Coord. Chem. Rev.* **2015**, *289–290*, 279–288; c) K. Mitchell, J. A. Ibers, *Chem. Rev.* **2002**, *102*, 1929–1952; d) H.-X. Li, Y.-J. Zhu, M.-L. Cheng, Z.-G. Ren, J.-P. Lang, Q. Shen, *Coord. Chem. Rev.* **2006**, *250*, 2059–2092; e) J. Lee, D. Freedman, J. H. Melman, M. Brewer, L. Sun, T. J. Emge, F. H. Long, J. G. Brennan, *Inorg. Chem.* **1998**, *37*, 2512–2519; f) A. C. Hillier, S.-Y. Liu, A. Sella, M. R. J. Elsegood, *Inorg. Chem.* **2000**, *39*, 2635–2644; g) F. Nief, *Coord. Chem. Rev.* **1998**, *178–180*, 13–81; h) W. J. Evans, K. A. Miller, D. S. Lee, J. W. Ziller, *Inorg. Chem.* **2005**, *44*, 4326–4332; i) S. Zitzer, T. Schleid, *Z. Anorg. Allg. Chem.* **2010**, *636*, 1050–1055; j) D. O. Charkin, C. Black, L. Downie, D. Sklovsky, P. S. Berdonosov, A. Olenev, W. Zhou, P. Lightfoot, V. A. Dolgikh, *J. Solid State Chem.* **2015**, *232*, 56–61; k) D. O. Charkin, S. Zitzer, S. Greiner, S. G. Dorofeev, A. V. Olenev, P. S. Berdonosov, T. Schleid, V. A. Dolgikh, *Z. Anorg. Allg. Chem.* **2017**, *643*, 1654–1660; l) D. R. Cary, J. Arnold, *Inorg. Chem.* **1994**, *33*, 1791–1796; m) D. R. Cary, G. E. Ball, J. Arnold, *J. Am. Chem. Soc.* **1995**, *117*, 3492–3501.
[4] D. V. Khasnis, M. Brewer, J. Lee, T. J. Emge, J. G. Brennan, *J. Am. Chem. Soc.* **1994**, *116*, 7129–7133.
[5] G. Thiele, S. Santner, C. Donsbach, M. Assmann, M. Muller, S. Dehnen, *Z. Kristallogr.* **2014**, *229*, 489–495.
[6] C. R. Groom, I. J. Bruno, M. P. Lightfoot, S. C. Ward, *Acta Crystallogr.* **2016**, *B72*, 171–179.
[7] D. J. Berg, R. A. Andersen, A. Zalkin, *Organometallics* **1988**, *7*, 1858–1863.
[8] Y.-Z. Ma, N. A. Pushkarevsky, T. S. Sukhikh, A. E. Galashov, A. G. Makarov, P. W. Roesky, S. N. Konchenko, *Eur. J. Inorg. Chem.* **2018**, 3388–3396.
[9] M. Brewer, D. Khasnis, M. Buretea, M. Berardini, T. J. Emge, J. G. Brennan, *Inorg. Chem.* **1994**, *33*, 2743–2747.
[10] a) C. O. Kienitz, C. Thöne, P. G. Jones, *Inorg. Chem.* **1996**, *35*, 3990–3997; b) G. Mugesh, H. B. Singh, R. J. Butcher, *J. Organomet. Chem.* **1999**, *577*, 243–248; c) G. Mugesh, H. B. Singh, R. J. Butcher, *Eur. J. Inorg. Chem.* **1999**, 1229–1236; d) G. Mugesh, H. B. Singh, P. R. Patel, R. J. Butcher, *Inorg. Chem.* **1998**, *37*, 2663–2669; e) Y. Cheng, T. J. Emge, J. G. Brennan, *Inorg. Chem.* **1996**, *35*, 7339–7344; f) Y. Cheng, T. J. Emge, J. G. Brennan, *Inorg. Chem.* **1994**, *33*, 3711–3714; g) V. K. Jain, *Dalton Trans.* **2020**, *49*, 8817–8835; h) M. A. Bhat, S. H. Lone, S. Ali, S. K. Srivastava, *J. Mol. Struct.* **2018**, *1171*, 233–242; i) G. Kedarnath, V. K. Jain, *Coord. Chem. Rev.* **2013**, *257*, 1409–1435; j) S. Patel, M. Meenakshi, A. S. Hodage, A. Verma, S. Agrawal, A. Yadav, S. Kumar, *Dalton Trans.* **2016**, *45*, 4030–4040; k) A. Pöllnitz, C. Silvestru, J.-F. Carpentier, A. Silvestru, *Dalton Trans.* **2012**, *41*, 5060–5070; l) R. K. Sharma, G. Kedarnath, A. Wadawale, V. K. Jain, B. Vishwanadh, *Inorg. Chim. Acta* **2011**, *365*, 333–339; m) A. Pöllnitz, A. Rotar, A. Silvestru, C. Silvestru, M. Kulcsar, *J. Organomet. Chem.* **2010**, *695*, 2486–2492; n) W.-F. Liaw, C.-H. Chen, G.-H. Lee, S.-M. Peng, *Organometallics* **1998**, *17*, 2370–2372; o) B. Mairychová, L. Dostál, A. Růžička, M. Fulem, K. Růžička, A. Lyčka, R. Jambor, *Organometallics* **2011**, *30*, 5904–5910.
[11] a) N. W. Alcock, *Adv. Inorg. Chem. Radiochem.* **1972**, *15*, 1–58; b) C. Bleiholder, D. B. Werz, H. Köppel, R. Gleiter, *J. Am. Chem. Soc.* **2006**, *128*, 2666–2674; c) C. Bleiholder, R. Gleiter, D. B. Werz, H. Köppel, *Inorg. Chem.* **2007**, *46*, 2249–2260; d) A. F. Cozzolino, P. J. W. Elder, I. Vargas-Baca, *Coord. Chem. Rev.* **2011**, *255*, 1426–1438; e) A. J. Mukherjee, S. S. Zade, H. B. Singh, R. B. Sunoj, *Chem. Rev.* **2010**, *110*, 4357–4416; f) D. J. Pascoe, K. B. Ling, S. L. Cockrof, *J. Am. Chem. Soc.* **2017**, *139*, 15160–15167; g) K. Selvakumar, H. B. Singh, *Chem. Sci.* **2018**, *9*, 7027–7042.
[12] R. Kaur, H. B. Singh, R. J. Butcher, *Organometallics* **1995**, *14*, 4755–4763.
[13] a) C. A. Collins, F. H. Fry, A. L. Holme, A. Yiakouvaki, A. Al-Qenaei, C. Pourzand, C. Jacob, *Org. Biomol. Chem.* **2005**, *3*, 1541–1546; b) S. Raju, H. B. Singh, S. Kumar, *Eur. J. Inorg. Chem.* **2022**, e202200300.
[14] R. D. Shannon, *Acta Crystallogr.* **1976**, *A32*, 751–767.
[15] J. Marçalo, A. P. De Matos, *Polyhedron* **1989**, *8*, 2431–2437.
[16] a) A. Pop, L. Wang, V. Dorcet, T. Roisnel, J.-F. Carpentier, A. Silvestru, Y. Sarazin, *Dalton Trans.* **2014**, *43*, 16459–16474; b) A. Pöllnitz, A. Rotar, A. Silvestru, C. Silvestru, M. Kulcsar, *J. Organomet. Chem.* **2010**, *695*, 2486–2492; c) R. Kaur, H. B. Singh, R. P. Patel, S. K. Kulshreshtha, *J. Chem. Soc. Dalton Trans.* **1996**, 461–466; d) R. D. Schluter, G. Kräuter, W. S. Rees Jr, *J. Cluster Sci.* **1997**, *8*, 123–154; e) L. Postigo, M. C. Maestre, M. E. G. Mosquera, T. Cuenca, G. Jiménez, *Organometallics* **2013**, *32*, 2618–2624; f) A. Gupta, R. Deka, R. J. Butcher, H. B. Singh, *Acta Crystallogr.* **2020**, *C76*, 828–835.
[17] M. J. Frisch, G. W. Trucks, H. B. Schlegel, G. E. Scuseria, M. A. Robb, J. R. Cheeseman, G. Scalmani, V. Barone, B. Mennucci, G. A. Petersson, H. Nakatsuji, M. Caricato, X. Li, H. P. Hratchian, A. F. Izmaylov, J. Bloino, G. Zheng, J. L. Sonnenberg, M. Hada, M. Ehara, K. Toyoto, R. Fukuda, J. Hasegawa, M. Ishida, T. Nakajima, Y. Honda, O. Kitao, H. Nakai, T. Vreven, J. A. Montgomery Jr, J. E. Peralta, F. Ogliaro, M. Bearpark, J. J. Heyd, E. Brothers, K. N. Kudin, V. N. Staroverov, R. Kobayashi, J. Normand, K. Raghavachari, A. Rendell, J. C. Burant, S. S. Iyengar, J. Tomasi, M. Cossi, N. Rega, J. M. Millam, M. Klene, J. E. Knox, J. B. Cross, V. Bakken, C. Adamo, J. Jaramillo, R. Gomperts, R. E. Stratmann, O. Yazyev, A. J. Austin, R. Cammi, C. Pomelli, J. W. Ochterski, R. L. Martin, K. Morokuma, V. G. Zakrzewski, G. A. Voth, P. Salvador, J. J. Dannenberg, S. Dapprich, A. D. Daniels, O. Farkas, J. B. Foresman, J. V. Ortiz, J. Cioslowski, D. J. Fox, *Gaussian 09, Revision A.02*, Gaussian, Inc., Wallingford CT, **2009**.
[18] A. D. Becke, *J. Chem. Phys.* **1993**, *98*, 5648–5652.
[19] T. H. Dunning Jr, P. J. Hay, *in Modern Theoretical Chemistry*, Ed. H. F. Schaefer III, Vol. 3 (Plenum, New York, **1977**) 1–28.
[20] A. Schäfer, C. Huber, R. Ahlrichs, *J. Chem. Phys.* **1994**, *100*, 5829–5835.
[21] T. R. Cundari, W. J. Stevens, *J. Chem. Phys.* **1993**, *98*, 5555–5565.
[22] E. D. Glendening, J. K. Badenhoop, A. E. Reed, J. E. Carpenter, J. A. Bohmann, C. M. Morales, C. R. Landis, F. Weinhold, *NBO 6.0*, Theoretical Chemistry Institute, University of Wisconsin, Madison, **2013**.
[23] A. D. Becke, K. E. Edgecombe, *J. Chem. Phys.* **1990**, *92*, 5397–5403.
[24] a) F. Biegler-König, J. Schönbohm, *J. Comput. Chem.* **2002**, *23*, 1489–1494; b) P. S. V. Kumar, V. Raghavendra, V. Subramanian, *J. Chem. Sci.* **2016**, *128*, 1527–1536; c) V. E. J. Berryman, J. J. Shephard, T. Ochiai, A. N. Price, P. L. Arnold, S. Parsons, N. Kaltsoyannis, *Phys. Chem. Chem. Phys.* **2020**, *22*, 16804–16812.
[25] a) J. Aihara, *J. Phys. Chem. A* **1999**, *103*, 7487–7495; b) S. K. Seth, D. K. Hazra, M. Mukherjee, T. Kar, *J. Mol. Struct.* **2009**, *936*, 277–282; c) S. K. Seth, N. C. Saha, S. Ghosh, T. Kar, *Chem. Phys. Lett.* **2011**, *506*, 309–314.
[26] a) G. Mugesh, H. B. Singh, *Acc. Chem. Res.* **2002**, *35*, 226–236; b) G. Kedarnath, V. K. Jain, *Coord. Chem. Rev.* **2013**, *257*, 1409–1435; c) S. C. Menon, H. B. Singh, J. M. Jasinski, J. P. Jasinski, R. J. Butcher, *Organometallics* **1996**, *15*, 1707–1712; d) G. Mugesh, A. Panda, S. Kumar, S. D. Apte, H. B. Singh, R. J. Butcher, *Organometallics* **2002**, *21*, 884–892; e) *The Chemistry of Organic Selenium and Tellurium Compounds*, ed. Z. Rappoport, John Wiley & Sons, Chichester, **2014**, vol. 4, Pt. 1.
[27] a) R. Sessolia, A. K. Powell, *Coord. Chem. Rev.* **2009**, *253*, 2328–2341; b) W. Boncher, H. Dalafu, N. Rosa, S. Stoll, *Coord. Chem. Rev.* **2015**, *289–290*, 279–288; c) B. Díaz, E. Granado, E. Abramof, P. H. O. Rappl, V. A. Chitta, A. B. Henriques, *Phys. Lett.* **2008**, *B 78*, 134423; d) A. B. Henriques, A. R. Naupa, P. A. Usachev, V. V. Pavlov, P. H. O. Rappl, E. Abramof, *Phys. Lett.* **2017**, *B 95*, 045205; e) A. B. Henriques, G. D. Galgano, E. Abramof, B. Diaz, P. H. O. Rappl, *Appl. Phys. Lett.* **2011**, *99*, 091906.
[28] T. Lu, F. Chen, *J. Comput. Chem.* **2012**, *33*, 580–592.
[29] N. P. Cowieson, D. Aragao, M. Clift, D. J. Ericsson, C. Gee, S. J. Harrop, N. Mudie, S. Panjikar, J. R. Price, A. Riboldi-Tunnicliffe, R. Williamson, T. Caradoc-Davies, *J. Synchrotron Radiat.* **2015**, *22*, 187–190.
[30] T. M. McPhillips, S. E. McPhillips, A. H.-J. Chiu, E. Cohen, A. M. Deacon, P. J. Ellis, E. Garman, A. Gonzalez, N. K. Sauter, R. P. Phizackerley, S. M. Soltis, P. Kuhn, *J. Synchrotron Radiat.* **2002**, *9*, 401–406.
[31] W. Kabsch, *J. Appl. Crystallogr.* **1993**, *26*, 795–800.
[32] a) G. M. Sheldrick, *Acta Crystallogr.* **2008**, *A64*, 112–122; b) G. M. Sheldrick, *Acta Crystallogr.* **2015**, *A71*, 3–8; c) G. M. Sheldrick, *Acta Crystallogr.* **2015**, *C71*, 3–8.
[33] O. V. Dolomanov, L. J. Bourhis, R. J. Gildea, J. A. K. Howard, *J. Appl. Crystallogr.* **2009**, *42*, 339–341.

Manuscript received: April 2, 2023
Accepted manuscript online: May 3, 2023
Version of record online: June 21, 2023